Spatial search by pseudo-Hermitian continuous-time quantum walks

Miaomiao Yu（余苗苗）,[1] **Yan Wang**（王焱）,[1] **Pingyu Zhu**（朱枰谕）,[1] **Kun Wang**（王琨）,[1] **and Ping Xu**（徐平）[1]

[1] College of Computer Science and Technology, National University of Defense Technology, Changsha 410073, China

E-mail: nju.wangkun@gmail.com

E-mail: pingxu520@nju.edu.cn

Abstract. We apply pseudo-Hermitian continuous-time quantum walks to the spatial search problem, derive exact analytical solutions for the resulting dynamics, and determine the first hitting time at which the target probability is maximal. In an idealized setting with a fixed coupling strength g, we show that the formal first-maximum time $t = \pi/g$ is independent of the database size N. However, we emphasize that this does not imply a general complexity improvement: making $t = \pi/g$ arbitrarily small requires a corresponding increase in the Hamiltonian matrix elements (energy scale), a fundamental resource trade-off. A fair assessment must also account for the measurement and postselection overhead required to extract the target probability and for the cost of implementing the evolution. Our results provide an analytically tractable non-Hermitian model that supports state preparation and parameter-controlled quantum dynamics.

Keywords: spatial search, pseudo-Hermitian quantum walk, continuous-time quantum walk, non-Hermitian Hamiltonian, quantum algorithm

PACS numbers: 03.67.Ac, 03.67.Lx, 03.65.Fd

1. Introduction

Since the pioneering work of Bender and Boettcher on non-Hermitian PT-symmetric quantum mechanics [1], there has been a surge of research exploring the mathematical properties of such systems and their potential physical applications [2, 3]. In Ref. [4], the authors consider a class of two-level Hermitian Hamiltonians and non-Hermitian PT-symmetric Hamiltonians. By calculating the evolution time from the initial state Ψ_I to the final state Ψ_F, they demonstrate that for a fixed energy constraint ω, the optimal evolution time τ under non-Hermitian dynamics can approach zero, provided the matrix elements of the non-Hermitian Hamiltonian are sufficiently large. They attribute this wormhole-like effect in Hilbert space to the fact that, while the initial and final states are orthogonal in the Hermitian case, they are instead separated by a finite angle in the non-Hermitian scenario. This faster-than-Hermitian evolution has subsequently been observed experimentally in a PT-symmetric system [5]. However, Ref. [6] challenges this interpretation, arguing that it remains unclear whether the result truly corresponds to arbitrarily close initial and final states. They claim that to rigorously establish the "faster-than-Hermitian" evolution, one must consider states with a fixed distance and determine whether the evolution time can indeed breach the fundamental bound imposed by Hermitian quantum mechanics.

Numerous studies have examined optimal evolution times for both Hermitian and non-Hermitian Hamiltonians [7, 8]. These studies motivate exploring how non-Hermitian dynamics affect quantum communication and search protocols. Motivated by this perspective, we apply pseudo-Hermitian continuous-time quantum walks (PHCTQWs) to the spatial search problem, focusing on the exactly solvable structure and the parameter-controlled dynamics of this setting. Below, we first review Grover's quantum search algorithm and the continuous-time quantum-walk (CTQW) spatial search algorithm, highlighting the physical intuition behind each. This intuition then motivates our construction of a spatial search algorithm based on PHCTQWs.

Grover's quantum search algorithm [9] implements a unitary evolution that transforms an initial state into the target solution state. The Grover iteration $G = (2|\psi\rangle\langle\psi| - I)O$, with phase oracle $O = I - 2|w\rangle\langle w|$, can be viewed as a rotation within the two-dimensional space spanned by the initial uniform superposition state $|\psi\rangle = \sum_x |x\rangle / \sqrt{N}$ and the target state $|w\rangle$ (which are not orthogonal but are linearly independent), taken here to represent a single marked item [10]. Grover iterations rotate $|\psi\rangle$ to $|w\rangle$, ensuring a high probability of success in finding a marked item when measured in the computational basis. Subsequently, an analog of Grover's algorithm was proposed [11], and was later related to CTQW spatial search [12]. This approach considers a simple Hamiltonian encoding $H^{CTQW} = |w\rangle\langle w| + |\psi\rangle\langle\psi|$ to solve the search problem. Notably, the optimal observation time t is independent of the specific marked element w. After a unitary evolution for time t, the final

state is $|\psi(t)\rangle = e^{-iH^{CTQW}t}|\psi\rangle$, and the probability of obtaining the target state $|w\rangle$ is given by:

$$p_w(t) = \sin^2\left(\frac{1}{\sqrt{N}}t\right) + \frac{1}{N}\cos^2\left(\frac{1}{\sqrt{N}}t\right). \tag{1}$$

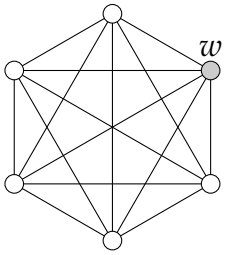
Measuring the system at time $t = \pi\sqrt{N}/2$ yields the target state $|w\rangle$ with probability one. Note that $|\psi\rangle\langle\psi| = (A+I)/N$, where A is the adjacency matrix of the loopless complete graph of size N. Using $-A/N - |w\rangle\langle w| = -H^{CTQW} + I/N$, the algorithm can be viewed as a spatial search algorithm on a complete graph. The identity term contributes only a global phase, while the sign reversal reverses time; for this real symmetric Hamiltonian and the specified real initial and target states, the transition probability is unchanged. See Figure 1(a) for an illustration on a six-vertex complete graph [12]. By using adjacency matrices of different graph structures, this algorithm can achieve spatial search on various types of graphs [12, 13]. Quantum walks on structured lattices further exhibit rich localization phenomena, such as the mobility edges and localization characteristics found in one-dimensional quasiperiodic quantum walks [14]. Both Grover's algorithm and the complete-graph CTQW search algorithm require $O(\sqrt{N})$ complexity and have been proven optimal [15, 13]. We therefore examine non-Hermitian quantum walks as a setting for exploring spatial search dynamics.

In the remainder of this work, we apply pseudo-Hermitian continuous-time quantum walks to the spatial search problem. We emphasize at the outset that our results do not constitute a general complexity improvement over the optimal $\Theta(\sqrt{N})$ quantum search: the constant-time scaling we report is an idealized property that holds for a fixed coupling strength g, and it is obtained only at the cost of a corresponding increase in the Hamiltonian's energy scale. More generally, for quantum-simulation-type algorithms of this kind, the evolution time is not the only figure of merit: a fair comparison must also account for the full resource budget, including the Hamiltonian energy scale and the measurement and postselection overhead required to extract the target probability. We therefore present our construction as an analytically tractable non-Hermitian model that supports state preparation and parameter-controlled quantum dynamics, rather than as an unconditional algorithmic speed-up.

2. Spatial search by pseudo-Hermitian quantum walk

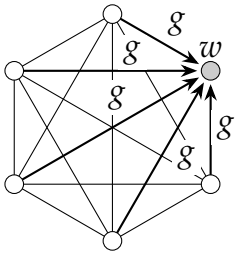
In this section, we first provide a formal description of the pseudo-Hermitian quantum walk. We then present our pseudo-Hermitian spatial search algorithm and determine the first maximum of its target probability. Finally, we discuss implementation considerations and outline potential applications.

(a) Hamiltonian encoding of CTQW search



$$\longrightarrow A = \begin{pmatrix} 0 & 1 & 1 & 1 & 1 & 1 \\ 1 & 0 & 1 & 1 & 1 & 1 \\ 1 & 1 & 0 & 1 & 1 & 1 \\ 1 & 1 & 1 & 0 & 1 & 1 \\ 1 & 1 & 1 & 1 & 0 & 1 \\ 1 & 1 & 1 & 1 & 1 & 0 \end{pmatrix} \longrightarrow H^{CTQW} = -\frac{A}{N} - |w\rangle\langle w|$$

(b) Hamiltonian encoding of our pseudo-Hermitian search



$$\longrightarrow A = \begin{pmatrix} 0 & g & g & g & g & g \\ 0 & 0 & 1 & 1 & 1 & 1 \\ 0 & 1 & 0 & 1 & 1 & 1 \\ 0 & 1 & 1 & 0 & 1 & 1 \\ 0 & 1 & 1 & 1 & 0 & 1 \\ 0 & 1 & 1 & 1 & 1 & 0 \end{pmatrix} \longrightarrow H = D - A$$

Figure 1. Hamiltonian encoding for quantum search algorithms on a six-vertex complete graph ($N = 6$). (a) The CTQW search algorithm typically encodes the Hamiltonian using the adjacency matrix A and the designated target vertex w. (b) The non-Hermitian quantum search algorithm encodes the marked vertex w through modified edge weights, leading to a weighted digraph structure characterized by the adjacency matrix A and the outdegree matrix D, where g is a tunable weight parameter. The first row and column of the displayed adjacency matrix correspond to the marked vertex w. For clarity, the directions and weights of non-target-related edges in the digraph are omitted.

2.1. Pseudo-Hermitian quantum walk

The essential idea is to utilize the pseudo-Hermitian continuous-time quantum walk (PHCTQW) scheme, which is reviewed in Appendix A and briefly summarized here. Let $\mathcal{H}$ be a finite-dimensional complex inner product space. A square linear operator $H : \mathcal{H} \to \mathcal{H}$ is said to be *pseudo-Hermitian* in the positive-metric sense used here if it has real eigenvalues and is diagonalizable [16, 17]. Let $H^\dagger$ be the conjugate transpose of H. When H is pseudo-Hermitian, there exists a positive-definite Hermitian linear automorphism operator Θ such that [16]

$$H^\dagger = \Theta H \Theta^{-1}. \tag{2}$$

Importantly, H is Hermitian with respect to the inner product $\langle \cdot | \Theta | \cdot \rangle$. A PHCTQW utilizes a pseudo-Hermitian H as its evolution Hamiltonian and operates as follows:

Given an initial system state $|\psi(0)\rangle$, the system's evolution is governed by the Schrödinger equation $i\hbar\frac{d}{dt}|\psi(t)\rangle = H|\psi(t)\rangle$. Solving this equation gives the output state at time t:

$$|\psi(t)\rangle = \sum_n e^{-iE_n t}|\psi_n\rangle\langle\phi_n|\psi(0)\rangle, \tag{3}$$

where we set $\hbar = 1$. Here, E_n and $|\psi_n\rangle$ are the nth eigenvalue and eigenvector of H, respectively, while E_n and $|\phi_n\rangle$ are the nth eigenvalue and eigenvector of $H^\dagger$, since the spectrum is real. The eigenbases are chosen biorthonormally, with $\langle\phi_m|\psi_n\rangle = \delta_{mn}$. Let $|w\rangle$ be a computational basis state. Define

$$p_w(t) := \frac{|\langle w|\sqrt{\Theta}|\psi(t)\rangle|^2}{\langle\psi(0)|\Theta|\psi(0)\rangle}. \tag{4}$$

The denominator equals $\langle\psi(t)|\Theta|\psi(t)\rangle$ by Θ-unitarity. The positive metric is not unique; here and below it is fixed by the biorthogonal eigenvectors normalized as in Appendix B. All metric-probability values quoted for this model refer to that choice. We prove in Appendix A that $\{p_w(t)\}_w$ constitutes a probability distribution, which we interpret as the transition probability of PHCTQW at vertex w and time t.

2.2. Spatial search by PHCTQW

We employ the above PHCTQW scheme for the spatial search problem. The key is to design a non-Hermitian Hamiltonian that encodes the search target. In conventional CTQW-based spatial search algorithms, the Hermitian Hamiltonian is encoded using the adjacency matrix A of the complete graph, along with a marked vertex w representing the target state. Inspired by non-Hermitian quantum mechanics, we construct a *non-Hermitian* Hamiltonian by modifying the edges incident on the marked vertex w. For $N \geq 2$ and $g > 0$, we modify the complete graph by: (1) modifying the (undirected) complete graph to a bidirectional complete graph with unit weight; (2) removing all outgoing edges from w; and (3) assigning a weight g to all its incoming edges. This construction results in a weighted digraph, whose Laplacian matrix is given by $L = D - A$, where A is the adjacency matrix and D is an $N \times N$ diagonal matrix with entries $D_{jj} := \sum_i A_{ij}$, representing the weighted outdegree of vertex j [18]. We adopt the convention that A_{ij} equals the weight of the edge $j \to i$. We utilize the Laplacian matrix as the Hamiltonian encoding of our search problem. Mathematically, the encoded Hamiltonian reads:

$$H := L = D - A = \begin{pmatrix} N+g-2 & -1 & \cdots & 0 & \cdots & -1 \\ -1 & N+g-2 & \cdots & 0 & \cdots & -1 \\ \vdots & \vdots & \ddots & \vdots & & \vdots \\ -g & -g & \cdots & 0 & \cdots & -g \\ \vdots & \vdots & & \vdots & \ddots & \vdots \\ -1 & -1 & \cdots & 0 & \cdots & N+g-2 \end{pmatrix}. \tag{5}$$

The Hamiltonian encoding process of a six-vertex complete graph is visualized in Figure 1(b).

Let us spell out this construction explicitly. With the convention that A_{ij} is the weight of the directed edge $j \to i$, the three modification steps yield an adjacency matrix whose w-th row and w-th column are distinguished: $A_{wj} = g$ for $j \neq w$ (the incoming edges of w carry weight g), $A_{iw} = 0$ for all i (all outgoing edges of w are removed), and $A_{ij} = 1$ for the remaining entries $i \neq j$ with $i, j \neq w$. The diagonal matrix D collects the weighted outdegrees, $D_{jj} = \sum_i A_{ij}$, so that $D_{jj} = N + g - 2$ for $j \neq w$ and $D_{ww} = 0$. Hence $H = D - A$ has diagonal entries $N + g - 2$ (for $j \neq w$) and 0 (for $j = w$), a w-th row equal to $-g$ off the diagonal, and a vanishing w-th column, as displayed in Eq. (5). The distinguished row and column therefore sit at the same index w: the $-g$ row and the vanishing column reflect, respectively, the weighted incoming edges and the removed outgoing edges of the marked vertex. In Fig. 1 the marked vertex is simply relabeled as vertex 1 for visualization, which is permissible because the complete graph is vertex-transitive. We also note that $g > 0$ is essential: it is the asymmetry between the w-th row (g) and the w-th column (0) that renders H non-Hermitian. Setting $g = 0$ removes the incoming edges as well, so A becomes symmetric and H reduces to the Hermitian Laplacian of the complete graph on the remaining $N - 1$ vertices with w completely decoupled; in this Hermitian limit no amplitude is transferred to w, so the marked-vertex probability remains at its initial uniform value $1/N$ rather than being amplified. We follow the Laplacian convention of Ref. [18] (the Hamiltonian is $D - A$ with D the weighted outdegree matrix); the specific weighted digraph, and hence the explicit form of A, is our own construction.

By inspection, the Hamiltonian H is non-Hermitian. We analytically compute its eigenvalues and eigenvectors in Appendix B, confirming that H possesses real eigenvalues and is diagonalizable, and is thus pseudo-Hermitian. If we configure the PHCTQW by setting the initial system state to the uniform superposition state and the evolution Hamiltonian to H, using the metric constructed in Appendix B, the probability distribution $p_w(t)$ defined in Eq. (4) simplifies to:

$$p_w(t) = \frac{(2N-1)\sqrt{N}+1}{2(2N-1)\sqrt{N}} + \frac{1-N}{2N-1}\cos(gt). \tag{6}$$

The derivation is available in Appendix B. Choosing the measurement time $t = \pi/g$ yields the target state $|w\rangle$ with a probability of:

$$p_w(\pi/g) = \frac{(4N-3)\sqrt{N}+1}{2(2N-1)\sqrt{N}} = \Theta(1). \tag{7}$$

Although $p_w(\pi/g) < 1$ for finite N, it approaches unity rapidly: $p_w(\pi/g) = 1 - \frac{1-1/\sqrt{N}}{4N-2}$, with its minimum at $N = 2$, where $p_w(\pi/g) \approx 0.951$. Thus $p_w(\pi/g) \geq 0.95$ for all $N \geq 2$. This is the metric probability of Eq. (4), not the conditional

probability of ordinary marked-vertex readout in the dilation protocol of Sec. 2.5. That protocol has conditional probability $q_w(\pi/g) = (2N-1)^2/[N(4N-3)]$ and per-attempt probability $P_w(\pi/g)$ given in Eq. (18). Its expected number of physical attempts is $1/P_w(\pi/g) = 1 + O(1/N)$; the expected sum of the simulated evolution intervals is therefore $O(1/g)$. The time needed to implement the dilation unitary is not determined by this trial count.

This result has two significant consequences: First, the required evolution time is independent of the problem size N, achieving a constant-time evolution for fixed g. Second, by experimentally tuning the non-Hermitian parameter g to a sufficiently large value, the evolution time $t = \pi/g$ can be made arbitrarily small, providing finer control over the formal evolution timescale.

However, we emphasize that these consequences do not amount to a general complexity improvement. The constant hitting time relies on g being a free parameter, and making $t = \pi/g$ arbitrarily small requires a corresponding increase in the Hamiltonian matrix elements (energy scale), representing a fundamental resource trade-off. This trade-off is discussed in light of the criticisms of non-Hermitian speed-ups in Ref. [6]. The constant-time scaling should therefore be read as an idealized property of the specified dynamics; our results are better viewed as a framework for spatial search dynamics and state preparation rather than an unconditional algorithmic speed-up.

We also note that our construction is specialized to the complete graph. The closed-form result for $p_w(t)$ and the ensuing hitting time $t = \pi/g$ rely on the high symmetry of the complete graph: because all unmarked vertices are equivalent, the $(N-2)$-dimensional zero-sum unmarked sector collapses into the single degenerate eigenvalue $N + g - 1$, while the remaining unmarked mode (the uniform superposition over unmarked vertices) participates in the active two-dimensional sector, so that the search dynamics is confined to the two-dimensional subspace associated with the eigenvalues 0 and g. For a general graph, one may define an analogous encoding, retaining the graph Laplacian and assigning weight g to the marked vertex's incoming edges, but the reduced symmetry no longer collapses the unmarked subspace, and no closed-form analytical solution is available in general. We therefore present our results as an analytically tractable non-Hermitian model of spatial search dynamics and state preparation, rather than as a general search algorithm for arbitrary graph families; extending the construction beyond complete graphs is an interesting direction for future work.

2.3. Hermitian counterpart

It is established by Mostafazadeh [19] that any pseudo-Hermitian Hamiltonian in this positive-metric class possesses an exact Hermitian counterpart. Appendix A provides its explicit construction. This correspondence allows us to map the non-Hermitian evolution onto an equivalent Hermitian formulation via a similarity

transformation. We emphasize that this equivalence is formal: it relates the dynamics under an appropriate change of representation (metric), and does not imply that the pseudo-Hermitian and Hermitian descriptions lead to the same operational performance or implementation cost under the standard inner product and measurement model. When initial states and observables are transformed consistently, the two representations give identical probabilities; the comparison below instead uses the same uniform initial vector in both representations.

Specifically, the Hermitian counterpart $\tilde{H}$ for the non-Hermitian Hamiltonian H given in Eq. (5) can be constructed via the similarity transformation:

$$\tilde{H} := \eta H \eta^{-1}, \tag{8}$$

where $\eta = \sqrt{\Theta}$. This counterpart uses the same fixed metric specified above; a different admissible metric generally gives a different counterpart. After a unitary evolution for time t under $\tilde{H}$, the final state is $|\tilde{\psi}(t)\rangle = e^{-i\tilde{H}t}|\psi(0)\rangle$, where $|\psi(0)\rangle$ is the same uniform initial vector used above. This constitutes a standard CTQW. The probability of observing the target state $|w\rangle$ at the time t is given by:

$$\tilde{p}_w(t) = |\langle w|\tilde{\psi}(t)\rangle|^2. \tag{9}$$

Solving the evolution yields:

$$\tilde{p}_w(t) = \frac{N+1}{2N} + \frac{1-N}{2N}\cos(gt). \tag{10}$$

Measuring the system in the computational basis at the specific time $t = \pi/g$ results in the target state $|w\rangle$ with unit probability. The detailed derivation can be found in Appendix C.

Remarkably, the time of the first probability maximum for the corresponding Hermitian Hamiltonian remains identical to that of the non-Hermitian system, while the fixed-metric probability p_w and the probability $\tilde{p}_w$ for the specified Hermitian input exhibit only minor quantitative differences. To further understand this distinction, we compare the amplitudes $\langle w|\sqrt{\Theta}|\psi(t)\rangle$ and $\langle w|\tilde{\psi}(t)\rangle$, which appear in Eqs. (4) and (9), respectively. Given the similarity transformation $\tilde{H} = \eta H \eta^{-1}$, $\tilde{H}$ and H share the same eigenvalues, and the eigenvectors of $\tilde{H}$ are $\{\eta|\psi_n\rangle\}_n$. Consequently, we have:

$$\langle w|\sqrt{\Theta}|\psi(t)\rangle = \sum_n e^{-iE_n t}\langle w|\eta|\psi_n\rangle\langle\phi_n|\psi(0)\rangle, \tag{11}$$

$$\langle w|\tilde{\psi}(t)\rangle = \sum_n e^{-iE_n t}\langle w|\eta|\psi_n\rangle\langle\psi_n|\eta|\psi(0)\rangle. \tag{12}$$

According to [20], for the metric in Eq. (A.6), the biorthogonal basis satisfies $|\phi_n\rangle = \Theta|\psi_n\rangle = \eta^2|\psi_n\rangle$. To ensure the success probability $p_w(t)$ defined in Eq. (4) matches the probability $\tilde{p}_w(t) = |\langle w|\tilde{\psi}(t)\rangle|^2$, one strategy is to apply the inverse metric operator η^{-1} to the initial state prior to the nonunitary evolution $U(t) = e^{-iHt}$. The resulting input has unit metric norm when the original input has unit ordinary norm.

2.4. First probability maximum

The equivalence between Hermitian and non-Hermitian quantum mechanics for pseudo-Hermitian Hamiltonians [19] not only provides a viable perspective for understanding the non-Hermitian search but also offers a clear framework for analyzing the evolution timescale in non-Hermitian dynamics [6]. For the specified Hamiltonians and initial states, Eqs. (6) and (10) show that the target probabilities have the form $a - b\cos(gt)$, with $b > 0$ for $N \geq 2$. Hence their first maxima occur when $gt = \pi$, giving $t = \pi/g$ for $g > 0$. The relevant two-level energy gap is g, as shown in Appendix C, consistent with this inverse-g timescale. This establishes the first maximum for the specified dynamics; it does not establish global time optimality or saturation of a geometric quantum speed limit [21, 22].

We now discuss the energy-scale trade-off underlying this $1/g$ timescale, which directly addresses the criticism of Ref. [6] concerning non-Hermitian speed-ups. The hitting time $t = \pi/g$ can be made arbitrarily small only by enlarging g, and since g enters H through its matrix elements (the diagonal entries are $N + g - 2$ and the entries of the marked row are $-g$), the spectral norm of the full Laplacian encoding is $\|H\| = \max\{g\sqrt{N}, N + g - 1\}$ for $N \geq 3$ (and $\|H\| = g\sqrt{2}$ for $N = 2$), growing at least linearly with both N and g. A shorter hitting time is thus purchased with a larger energy scale for this encoding. Under a fixed energy budget $\|H\| \leq E$, the largest eigenvalue $N + g - 1$ (for $N \geq 3$) gives $g \leq E - N + 1$, so a positive gap is available only for $N < E + 1$; the database size is bounded by the available energy for this full Hamiltonian. The constant-time scaling is therefore a resource trade-off rather than a violation of the $\Theta(\sqrt{N})$ lower bound, in agreement with the resolution of Ref. [6] that a genuine speed-up must account for the energy resources.

2.5. Physical implementation

To physically implement our algorithm, two experimental capabilities are required: (i) realizing evolution generated by a non-Hermitian Hamiltonian, and (ii) estimating the time-dependent probability $p_w(t)$ through appropriate measurements and data processing.

Two complementary routes are available for implementing the non-Hermitian evolution. The first is *direct engineering* of a platform whose effective dynamics are governed by the desired non-Hermitian Hamiltonian, with photonic systems providing a natural example. As demonstrated in [23], when a non-Hermitian Hamiltonian H is diagonalizable one may write

$$H = PH_dP^{-1}, \quad U(t) = e^{-iHt} = Pe^{-iH_dt}P^{-1}, \tag{13}$$

where H_d is diagonal and P contains the nonorthogonal eigenvectors. In the pseudo-Hermitian regime, the spectrum is real, so e^{-iH_dt} corresponds to diagonal phase accumulation as in standard CTQW, while the nonunitary basis-change operations P and P^{-1} capture the genuinely non-Hermitian structure. Ref. [23] implemented

such nonunitary operations by enlarging the photonic Hilbert space and introducing controlled loss, an approach that can be adapted to realize the evolution required here.

The second route is to *simulate* the non-Hermitian dynamics using an overall Hermitian system. Experimentally, an arbitrary nonunitary evolution can be implemented via unitary dilation with ancillas and postselection [24]. Alternatively, one may simulate the dynamics through the Hermitian counterpart obtained by a similarity transformation (e.g., $\tilde{H} = \eta H \eta^{-1}$, with η determined by the metric) [25]. Beyond photonics, superconducting circuits [26] and cold-atom platforms [27] also offer potential platforms for investigating the implementation of the required dynamics. Finally, the extensive experimental literature on both Hermitian quantum walks [28, 29, 30, 31, 32, 33] and non-Hermitian quantum walks [34, 35, 36, 37, 38] demonstrates several relevant experimental ingredients for non-Hermitian quantum-walk dynamics. On the trapped-ion platform, a scheme for realizing the two-dimensional non-Hermitian skin effect through a discrete-time quantum walk with a single trapped ion has recently been proposed [39].

We next address how to estimate the time-dependent success probability. Ideally, a pseudo-Hermitian platform would provide a direct measurement of the outcome distribution, analogous to computational-basis readout in CTQW. In current experimental realizations, however, the non-Hermitian evolution e^{-iHt} is typically implemented only as an *effective* evolution, obtained either by controlled loss or by postselection through unitary dilation.

In the controlled loss approach [23], the nonunitary evolution manifests as effective dynamics conditioned on detection ("survival"). Let $C_j(t)$ denote the detected counts in output mode j at evolution time t. The experimentally inferred distribution is obtained by normalization,

$$q_w(t) = \frac{C_w(t)}{\sum_{j=1}^{N} C_j(t)}, \tag{14}$$

where $q_w(t) = |\langle w|\psi(t)\rangle|^2 / \langle \psi(t)|\psi(t)\rangle$. The dilation protocol analyzed below uses this ordinary graph-sector readout without a metric filter. It therefore measures $q_w(t)$ conditional on retaining the system branch, rather than the metric probability $p_w(t)$ of Eq. (4).

In the unitary-dilation approach [24], the system undergoes a joint unitary evolution on the system and an ancilla, and the effective nonunitary map is obtained by conditioning on a designated ancilla outcome. The success probability of such a protocol is the product of the postselection probability of that outcome and the conditional probability of detecting the walker at the marked vertex; we evaluate both explicitly for a specific realization below.

We now specify one protocol explicitly and calculate its postselection and readout probabilities. We adopt the unitary-dilation construction of Ref. [24], in which the $N \times N$ nonunitary evolution operator $G(t) = e^{-iHt}$ is embedded in a

$2N \times 2N$ unitary operator,

$$U_A(t) = \begin{pmatrix} \dfrac{G(t)}{\lambda(t)} & \sqrt{1 - \dfrac{G(t)G^\dagger(t)}{\lambda^2(t)}} \\ \sqrt{1 - \dfrac{G^\dagger(t)G(t)}{\lambda^2(t)}} & -\dfrac{G^\dagger(t)}{\lambda(t)} \end{pmatrix}, \quad \lambda(t) \equiv \sqrt{\max_k \lambda_k(t)} = \|G(t)\|, \tag{15}$$

where $\lambda_k \geq 0$ are the eigenvalues of $G(t)G^\dagger(t)$. Scaling by the operator norm $\|G(t)\|$ renders the defect operator $1 - G(t)G^\dagger(t)/\|G(t)\|^2$ nonnegative, and hence $U_A(t)$ unitary. The graph state is embedded in the enlarged Hilbert space as $|\Psi(0)\rangle = (|\psi_s(0)\rangle, |0\rangle)^T$ with $|\psi_s(0)\rangle = |s\rangle$, so that the walker starts on the graph while the environment register is empty; the protocol consists of preparing this state, applying $U_A(t)$, and measuring all $2N$ modes.

Since the upper-left block of Eq. (15) carries the scaled evolution, the system component of the evolved state is $|\psi_s(t)\rangle = G(t)|s\rangle / \|G(t)\|$, and the probability of finding the walker in the system sector—rather than in the environment, whose population is the signature of the nonunitary evolution on the graph—is

$$P_{\text{sys}}(t) = \| \, |\psi_s(t)\rangle \, \|^2 = \frac{\langle s|G^\dagger(t)G(t)|s\rangle}{\|G(t)\|^2}. \tag{16}$$

The two ingredients of Eq. (16) are fixed by the full $N \times N$ matrices. On the unmarked zero-sum subspace the eigenvalue $N + g - 1$ is $(N-2)$-fold degenerate with $|\phi_p\rangle = |\psi_p\rangle$, so $N-2$ singular values of $G(t)$ equal unity and only the remaining two-dimensional block $B(t)$ can exceed one. Its two eigenvalues follow from the full-matrix trace and determinant,

$$\operatorname{tr}\left[G^\dagger(t)G(t)\right] = 3N - 2 - 2(N-1)\cos(gt), \qquad \det\left[G^\dagger(t)G(t)\right] = |\det G(t)|^2 = 1,$$

the determinant being unit because $G(t) = e^{-iHt}$ and the spectrum of H is real. Hence the two non-unit eigenvalues λ satisfy $\lambda^2 - \operatorname{tr}[B(t)]\,\lambda + 1 = 0$ with $\operatorname{tr} B(t) = 2N - 2(N-1)\cos(gt)$, and at $t = \pi/g$,

$$\lambda_{\max}\left(G^\dagger G\right) = \frac{4N - 2 + \sqrt{(4N-2)^2 - 4}}{2} = \left(\sqrt{N} + \sqrt{N-1}\right)^2.$$

Combined with $\langle s|G^\dagger(\pi/g)G(\pi/g)|s\rangle = 4N - 3$ from Eq. (B.11), Eq. (16) gives $P_{\text{sys}}(\pi/g) = (4N-3)/(\sqrt{N} + \sqrt{N-1})^2 = 1 - 1/(4N-2) + O(N^{-2})$, approaching unity: the postselection that restricts the readout to the graph is essentially free.

Completing the protocol by measuring the walker in the graph sector, the end-to-end probability of detecting it at the marked vertex is

$$P_w(t) = \left| \langle w| \frac{G(t)}{\|G(t)\|} |s\rangle \right|^2 = \frac{(2N-1)^2 - 4N(N-1)\cos^2(gt/2)}{N\,\|G(t)\|^2}, \tag{17}$$

so that at $t = \pi/g$

$$P_w(\pi/g) = \frac{(2N-1)^2}{N\left(\sqrt{N}+\sqrt{N-1}\right)^2} = 1 - \frac{1}{2N} + O\left(N^{-2}\right). \tag{18}$$

This is the success probability per physical attempt for ordinary marked-vertex readout, without metric filtering. Conditional on finding the walker in the graph sector, the corresponding probability is $q_w(\pi/g) = P_w(\pi/g)/P_{\mathrm{sys}}(\pi/g) = (2N-1)^2/[N(4N-3)]$, which differs from $p_w(\pi/g)$ at finite N. The time $t = \pi/g$ is also the first positive-time maximum of $P_w(t)$: with $x(t) = \|G(t)\|^{-2}$, Eqs. (17) and the singular-value calculation above give $P_w(t) = 1 - (2 - 1/N)x(t) + x(t)^2$. On $0 \le t \le \pi/g$, $x(t)$ decreases from 1 to its value at π/g; this convex quadratic is maximized at an endpoint, and $P_w(\pi/g) > P_w(0) = 1/N$ for $N \ge 2$.

If the metric probability $p_w(t)$ itself is to be sampled, a different, sequential readout applies $K = \sqrt{\Theta}/\|\sqrt{\Theta}\|$ to the normalized system state after the successful dilation branch. At $t = \pi/g$, its conditional filter probability is

$$\begin{aligned} P_{\mathrm{filt|sys}}(\pi/g) &= \frac{\langle s|\Theta|s\rangle}{\|\Theta\|\,\langle s|G^\dagger(\pi/g)G(\pi/g)|s\rangle} \\ &= \frac{2N-1}{(4N-3)\sqrt{N}\left(\sqrt{N}+\sqrt{N-1}\right)} \\ &= \frac{1}{4N} + O(N^{-2}), \end{aligned} \tag{19}$$

where $\langle s|\Theta|s\rangle = (2N-1)/\sqrt{N}$ and $\|\Theta\| = \sqrt{N}+\sqrt{N-1}$ follow from Appendix B. The joint probability of the dilation branch, the metric filter, and a marked outcome is therefore

$$\begin{aligned} P_w^{(\mathrm{metric})}(\pi/g) &= P_{\mathrm{sys}}(\pi/g)P_{\mathrm{filt|sys}}(\pi/g)p_w(\pi/g) \\ &= \frac{(2N-1)p_w(\pi/g)}{\sqrt{N}\left(\sqrt{N}+\sqrt{N-1}\right)^3} \\ &= \frac{1}{4N} + O(N^{-2}). \end{aligned} \tag{20}$$

Thus the unfiltered search protocol requires $1/P_w(\pi/g) = 1 + O(1/N)$ physical attempts, whereas sampling a marked outcome of the metric distribution by this sequential filter requires $O(N)$ attempts. In the unfiltered protocol, each attempt uses the dilation corresponding to the simulated interval $t = \pi/g$, so the expected sum of such intervals is $O(1/g)$. The dilation identity does not specify the gate count or physical time required to implement $U_A(t)$; no end-to-end implementation-time scaling follows from the trial count alone.

2.6. Potential applications

We envision potential applications of our PHCTQW-based spatial search framework. More generally, the value of exactly solvable non-Hermitian models can lie in

their utility for near-term quantum tasks. Owing to its simple structure and analytically tractable spectrum, the Hamiltonian considered here may be useful beyond spatial search in at least two respects. First, it provides a natural mechanism for *state preparation*. The target state $|w\rangle$ appears as a distinguished eigenstate of the effective generator, so that appropriately engineered evolution, either in a controlled nonunitary setting or via an embedding into an open-system realization, can preferentially populate $|w\rangle$. In this way, the same ingredients used for search can be repurposed as a state-preparation primitive, where the dynamics concentrate amplitude on a desired computational-basis state. Beyond search and state preparation, the time evolution of pseudo-Hermitian Hamiltonians has recently been applied to quantum state discrimination [40, 41], pointing to a broader scope for exactly solvable non-Hermitian models of the kind considered here. Spatial-search-type weighting has likewise been applied beyond database search, for instance to extract information contained in cell-velocity distributions [42]. Second, the *tunability of* g offers an additional handle for controlling and probing the dynamics. In the pseudo-Hermitian regime, varying g directly adjusts the relevant dynamical timescale while preserving the analytic solvability of the model, which can be advantageous for calibration and benchmarking in experiments. More broadly, allowing g to take complex values moves the system beyond pseudo-Hermiticity into generic non-Hermitian dynamics; the resulting, still analytically tractable spectrum provides a convenient testbed for studying effective nonunitary control protocols in settings relevant to quantum information processing and photonic platforms.

2.7. Comparison with existing works

Several works have explored modified quantum-walk and non-Hermitian approaches to quantum search, and it is instructive to compare them along three axes: the assumptions made, the resources required, and the resulting scaling. We focus on two representative schemes.

Wong studied quantum walk search with time-reversal-symmetry breaking via a modified Hermitian graph Laplacian and reported a runtime of $O(\sqrt{N})$ with success probability approaching unity [43]. This scheme is Hermitian and unitarily implemented, so it requires no postselection, and its energy scale is $O(1)$: in the standard CTQW search construction, the graph term is rescaled by a coupling of order $1/N$ so that it and the oracle term have comparable, bounded magnitude. It thus attains the optimal $\Theta(\sqrt{N})$ scaling at unit energy scale and provides the natural benchmark against which faster-than-$\sqrt{N}$ claims should be measured.

Nesterov and Berman proposed a non-Hermitian adiabatic search scheme reporting an $O(\ln N)$ evolution-time scaling, compared with the $O(N)$ global and $O(\sqrt{N})$ local Hermitian adiabatic schedules [44]. These are reported evolution-time scalings for different models. A resource-matched comparison would also require

their Hamiltonian energy scales, success probabilities, and implementation costs to be accounted for on the same footing [6]. We do not calculate these resources for Nesterov and Berman's scheme, and thus draw no conclusion about its end-to-end performance.

For our construction, the formal hitting time is $t = \pi/g$ for fixed g. This scaling is purchased by (i) specializing to the complete graph, whose symmetry reduces the dynamics to a two-dimensional subspace, (ii) making g a free tunable parameter, and (iii) allowing the energy scale $\|H\| = \max\{g\sqrt{N}, N + g - 1\}$ for $N \geq 3$ (and $\|H\| = g\sqrt{2}$ for $N = 2$) to grow with N and g. The contrast with Wong's scheme is sharp: his $O(\sqrt{N})$ runtime is obtained at unit energy scale, whereas our energy scale grows linearly with N at fixed g. Indeed, if our Hamiltonian is normalized to unit energy, $H \to H/\|H\|$, then for fixed g and large N (where $\|H\| = N + g - 1$) the gap becomes $g/(N + g - 1)$ and the hitting time in the normalized units becomes $\pi(N + g - 1)/g = O(N)$, so the constant-time scaling is a resource artifact rather than a violation of the $\Theta(\sqrt{N})$ lower bound. The dilation of Sec. 2.5 requires $O(1)$ attempts for ordinary marked-vertex readout, but its gate count and implementation time have not been established. Our results are therefore best viewed not as a faster search algorithm, but as an analytically tractable pseudo-Hermitian model in which this resource trade-off can be made explicit. For $N \geq 3$, the $N + g - 1$ eigenvalue belongs to the unmarked zero-sum sector, which the uniform input does not populate. Thus the $O(N)$ unit-norm time pertains to this full Laplacian encoding and is not an implementation lower bound for every operator reproducing the evolution from the uniform input.

3. Conclusions

We applied pseudo-Hermitian continuous-time quantum walks to the spatial search problem and obtained an exact analytical solution. We established that $t = \pi/g$ is the first time at which the target probability is maximal for the specified dynamics. We also outlined experimental implementation proposals and potential applications based on current quantum technologies. Notably, the formal first-maximum time scales inversely with the tunable non-Hermitian parameter g, providing additional flexibility for experimental control. The unfiltered dilation has $O(1)$ expected trials, but its gate count and physical implementation time are not determined here. Moreover, shrinking $t = \pi/g$ requires enlarging g and hence the Hamiltonian's energy scale. The inverse-g evolution timescale is therefore an idealized resource trade-off, not a general complexity improvement. Our algorithm was formulated for complete graphs; extending the approach to more general graph families remains an interesting direction for future work. Overall, the value of our work lies not in a complexity advantage but in its providing an analytically tractable non-Hermitian model, a mechanism for state preparation, and parameter-controlled quantum dynamics, thereby offering a new perspective on spatial search tasks.

Acknowledgments

This work was supported by the National Key R&D Program of China (Grant No. 2022YFF0712800).

References

[1] Bender C M and Boettcher S 1998 *Physical Review Letters* **80** 5243
[2] El-Ganainy R, Makris K G, Khajavikhan M, Musslimani Z H, Rotter S and Christodoulides D N 2018 *Nature Physics* **14** 11–19
[3] Bender C M and Hook D W 2024 *Reviews of Modern Physics* **96** 045002
[4] Bender C M, Brody D C, Jones H F and Meister B K 2007 *Physical Review Letters* **98** 040403
[5] Zheng C, Hao L and Long G L 2013 *Philosophical Transactions of the Royal Society A: Mathematical, Physical and Engineering Sciences* **371** 20120053
[6] Mostafazadeh A 2007 *Physical Review Letters* **99** 130502
[7] Bender C M and Brody D C 2009 Optimal time evolution for Hermitian and non-Hermitian Hamiltonians *Time in Quantum Mechanics* (Springer) pp 341–361
[8] Mostafazadeh A 2009 *Physical Review A* **79** 014101
[9] Grover L K 1997 *Physical Review Letters* **79** 325
[10] Nielsen M A and Chuang I L 2010 *Quantum Computation and Quantum Information* (Cambridge University Press)
[11] Farhi E and Gutmann S 1998 *Physical Review A* **57** 2403
[12] Childs A M and Goldstone J 2004 *Physical Review A* **70** 022314
[13] Chakraborty S, Novo L, Ambainis A and Omar Y 2016 *Physical Review Letters* **116** 100501
[14] Cui X H, Wang H M and Li Z J 2024 *Chinese Physics B* **33** 060301
[15] Zalka C 1999 *Physical Review A* **60** 2746
[16] Mostafazadeh A 2002 *Journal of Mathematical Physics* **43** 205–214
[17] Mostafazadeh A 2002 *Journal of Mathematical Physics* **43** 2814–2816
[18] Wong T G, Tarrataca L and Nahimov N 2016 *Quantum Information Processing* **15** 4029–4048
[19] Mostafazadeh A 2003 *Journal of Physics A: Mathematical and General* **36** 7081
[20] Znojil M 2007 *arXiv preprint arXiv:0710.5653*
[21] Anandan J and Aharonov Y 1990 *Physical Review Letters* **65** 1697
[22] Carlini A, Hosoya A, Koike T and Okudaira Y 2006 *Physical Review Letters* **96** 060503
[23] Wu T, Izaac J, Li Z X, Wang K, Chen Z Z, Zhu S, Wang J and Ma X S 2020 *Physical Review Letters* **125** 240501
[24] Wang K, Shi Y, Xiao L, Wang J, Joglekar Y N and Xue P 2020 *Optica* **7** 1524–1530
[25] Izaac J, Wang J, Abbott P and Ma X 2017 *Physical Review A* **96** 032305
[26] Clarke J and Wilhelm F K 2008 *Nature* **453** 1031–1042
[27] Bloch I 2005 *Nature Physics* **1** 23–30
[28] Karski M, Förster L, Choi J M, Steffen A, Alt W, Meschede D and Widera A 2009 *Science* **325** 174–177
[29] Peruzzo A, Lobino M, Matthews J C, Matsuda N, Politi A, Poulios K, Zhou X Q, Lahini Y, Ismail N, Wörhoff K *et al.* 2010 *Science* **329** 1500–1503
[30] Broome M A, Fedrizzi A, Lanyon B P, Kassal I, Aspuru-Guzik A and White A G 2010 *Physical Review Letters* **104** 153602
[31] Schreiber A, Gábris A, Rohde P P, Laiho K, Štefaňák M, Potoček V, Hamilton C, Jex I and Silberhorn C 2012 *Science* **336** 55–58
[32] Qiang X, Wang Y, Xue S, Ge R, Chen L, Liu Y, Huang A, Fu X, Xu P, Yi T *et al.* 2021 *Science Advances* **7** eabb8375

[33] Wang Y, Yu X, Xue S, Wang Y, Zhan J, Wu C, Zhu P, Zheng Q, Yu M, Liu Y *et al.* 2022 *Science China Physics, Mechanics & Astronomy* **65** 100362
[34] Helbig T, Hofmann T, Imhof S, Abdelghany M, Kiessling T, Molenkamp L, Lee C, Szameit A, Greiter M and Thomale R 2020 *Nature Physics* **16** 747–750
[35] Wu Y, Liu W, Geng J, Song X, Ye X, Duan C K, Rong X and Du J 2019 *Science* **364** 878–880
[36] Weidemann S, Kremer M, Helbig T, Hofmann T, Stegmaier A, Greiter M, Thomale R and Szameit A 2020 *Science* **368** 311–314
[37] Regensburger A, Bersch C, Miri M A, Onishchukov G, Christodoulides D N and Peschel U 2012 *Nature* **488** 167–171
[38] Rüter C E, Makris K G, El-Ganainy R, Christodoulides D N, Segev M and Kip D 2010 *Nature Physics* **6** 192–195
[39] Hou W, Tang H, Xu Q and Lin Y 2024 *Chinese Physics Letters* **41** 040301
[40] Dong Q, Gao X, Liu Z, Li H, Wen J and Zheng C 2025 *Entropy* **27** 836
[41] Dong Q, Liu Z and Zheng C 2026 *Scientific Reports* **16** 13586
[42] Ma Y, Li N and Chen W 2024 *Chinese Physics B* **33** 028703
[43] Wong T G 2015 *Journal of Physics A: Mathematical and Theoretical* **48** 405303
[44] Nesterov A I and Berman G P 2012 *Physical Review A* **86** 052316
[45] Salimi S and Sorouri A 2010 *Journal of Physics A: Mathematical and Theoretical* **43** 275304

Supplemental Material for "Spatial search by pseudo-Hermitian continuous-time quantum walks"

A. Pseudo-Hermitian continuous-time quantum walks

This section briefly reviews the pseudo-Hermitian continuous-time quantum walks (PHCTQWs) initially proposed in [45]. PHCTQWs use pseudo-Hermitian operators constructed from directed graphs to enable the implementation of directed quantum walks. We first formally define the pseudo-Hermitian Hamiltonians.

Pseudo-Hermitian Hamiltonians. Let $\mathcal{H}$ be a finite-dimensional complex inner product space. A square linear operator $H : \mathcal{H} \to \mathcal{H}$ is said to be *pseudo-Hermitian* [16] if there exists a positive-definite Hermitian linear automorphism operator Θ such that

$$H^\dagger = \Theta H \Theta^{-1}, \tag{A.1}$$

where $H^\dagger$ is the conjugate transpose of H. Notably, it has been shown that H is actually a Hermitian operator with respect to the following positive-definite inner product:

$$\langle \cdot | \Theta | \cdot \rangle. \tag{A.2}$$

Mostafazadeh [16, 17] established the following two equivalent characterizations, which are restated in the quantum-walk setting by Izaac *et al.* [25]:

- H is pseudo-Hermitian if and only if it has real eigenvalues and is diagonalizable.
- H is pseudo-Hermitian if and only if there exists an invertible Hermitian operator η such that $\eta H \eta^{-1}$ is Hermitian.

This first characterization offers a quick way to verify if a given operator is pseudo-Hermitian, as a matrix is diagonalizable if and only if it possesses a complete set of linearly independent eigenvectors. The second characterization gives a similarity transformation to a Hermitian operator.

The question that arises is how to identify Θ and η given a pseudo-Hermitian operator H. A systematic construction is described in [25] and is briefly summarized here for completeness. Since H is pseudo-Hermitian, it must admit the following biorthonormal system of eigenvectors [16]

$$H |\psi_n\rangle = E_n |\psi_n\rangle , \tag{A.3}$$

$$H^\dagger |\phi_n\rangle = E_n |\phi_n\rangle , \tag{A.4}$$

where $\{E_n \in \mathbb{R}\}_n$ are the real eigenvalues of H and $H^\dagger$ (thanks to the first characterization, we know that H possesses real eigenvalues), and $\{|\psi_n\rangle\}_n$ and $\{|\phi_n\rangle\}_n$ are the eigenbases of H and $H^\dagger$, respectively. Notably, the state set $\{|\psi_n\rangle, |\phi_n\rangle\}_n$ forms a biorthonormal system satisfying $\langle\psi_m|\phi_n\rangle = \delta_{mn}$, where δ_{mn} is the Kronecker delta function. The completeness relation is given by $I = \sum_n |\psi_n\rangle\langle\phi_n|$. Then, the Hermitian operator η and its inverse η^{-1} can be constructed as follows:

$$\eta = \sqrt{\sum_n |\phi_n\rangle\langle\phi_n|}, \quad \eta^{-1} = \sqrt{\sum_n |\psi_n\rangle\langle\psi_n|}. \tag{A.5}$$

Based on this construction, it was proven in Eqs. (1)-(8) of Ref. [19] that $\tilde{H} = \eta H \eta^{-1}$ is indeed Hermitian. Furthermore, the Hermitian linear automorphism operator Θ can be chosen as

$$\Theta = \eta^2 = \sum_n |\phi_n\rangle\langle\phi_n|, \quad \Theta^{-1} = (\eta^{-1})^2 = \sum_n |\psi_n\rangle\langle\psi_n|. \tag{A.6}$$

PHCTQW. As the name indicates, PHCTQW is a continuous-time quantum walk whose evolution Hamiltonian H is pseudo-Hermitian, a fundamental departure from the Hermitian Hamiltonians employed in conventional continuous-time quantum walks. Specifically, for a pseudo-Hermitian time-independent Hamiltonian H and an initial system state $|\psi(0)\rangle$, the system's evolution is governed by the Schrödinger equation:

$$i\hbar \frac{d}{dt} |\psi(t)\rangle = H |\psi(t)\rangle . \tag{A.7}$$

Solving Eq. (A.7) gives the output state at time t,

$$|\psi(t)\rangle = \sum_n e^{-iE_n t} |\psi_n\rangle\langle\phi_n|\psi(0)\rangle, \tag{A.8}$$

where we assume $\hbar = 1$. From this equation it is evident that the eigenvalues and eigenvectors of H are essential. We can verify that the norm of the system state is conserved with respect to (w.r.t.) the inner product $\langle\cdot|\Theta|\cdot\rangle$:

$$\begin{aligned}
\langle\psi(t)|\Theta|\psi(t)\rangle &= \sum_{m,n} e^{-i(E_n - E_m)t} \langle\psi_m|\Theta|\psi_n\rangle\langle\psi(0)|\phi_m\rangle\langle\phi_n|\psi(0)\rangle && \text{(A.9)}\\
&= \sum_n e^{-i(E_n - E_n)t} \langle\psi_n|\phi_n\rangle\langle\psi(0)|\phi_n\rangle\langle\phi_n|\psi(0)\rangle && \text{(A.10)}\\
&= \langle\psi(0)| \left(\sum_n |\phi_n\rangle\langle\phi_n| \right) |\psi(0)\rangle && \text{(A.11)}\\
&= \langle\psi(0)|\Theta|\psi(0)\rangle, && \text{(A.12)}
\end{aligned}$$

where the second equality follows from Eq. (A.6) and the biorthonormality property $\langle\psi_m|\phi_n\rangle = \delta_{mn}$. Note that the value of $\langle\psi(0)|\Theta|\psi(0)\rangle$ is determined by the specific

initial state $|\psi(0)\rangle$ and is not 1 in general. The above equation shows that this inner product is conserved during system evolution.

To obtain a normalized transition-probability distribution, the conserved metric norm must be set to unity. Accordingly, the input state $|\psi(0)\rangle$ of the particle must be normalized w.r.t. the inner product $\langle\cdot|\Theta|\cdot\rangle$, yielding the "normalized" initial system state:

$$|\psi_0\rangle = \frac{|\psi(0)\rangle}{\sqrt{\langle\psi(0)|\Theta|\psi(0)\rangle}}. \tag{A.13}$$

Only for the following normalization argument, we write $|\psi(t)\rangle = e^{-iHt}|\psi_0\rangle$ for evolution from the metric-normalized input, rather than the input $|\psi(0)\rangle$ of Eq. (A.8). We can then see that the total transition probability of PHCTQW is indeed conserved:

$$\begin{aligned}\langle\psi(t)|\Theta|\psi(t)\rangle = \langle\psi_0|\Theta|\psi_0\rangle &= \frac{\langle\psi(0)|}{\sqrt{\langle\psi(0)|\Theta|\psi(0)\rangle}}\Theta\frac{|\psi(0)\rangle}{\sqrt{\langle\psi(0)|\Theta|\psi(0)\rangle}} \\ &= \frac{\langle\psi(0)|\Theta|\psi(0)\rangle}{\langle\psi(0)|\Theta|\psi(0)\rangle} = 1.\end{aligned} \tag{A.14}$$

Transition probability. Now that the total transition probability of PHCTQW is indeed conserved, we *define* the transition probability of PHCTQW at the vertex w and the time t as:

$$p_w(t) := |\langle w|\eta|\psi(t)\rangle|^2. \tag{A.15}$$

Under this definition, we can prove that $\{p_w(t)\}_w$ is indeed a probability distribution, given that each $p_w(t)$ is non-negative and their sum is normalized to 1:

$$\sum_w p_w(t) = \sum_w |\langle w|\eta|\psi(t)\rangle|^2 \tag{A.16}$$

$$= \sum_w \langle\psi(t)|\eta^\dagger|w\rangle \times \langle w|\eta|\psi(t)\rangle \tag{A.17}$$

$$= \langle\psi(t)|\eta^\dagger\left(\sum_w |w\rangle\langle w|\right)\eta|\psi(t)\rangle \tag{A.18}$$

$$= \langle\psi(t)|\Theta|\psi(t)\rangle \tag{A.19}$$

$$= \langle\psi_0|\Theta|\psi_0\rangle \tag{A.20}$$

$$= 1. \tag{A.21}$$

To simplify the formulation, we can avoid explicitly introducing the so-called "normalized" initial system state $|\psi_0\rangle$ by returning to $|\psi(t)\rangle = e^{-iHt}|\psi(0)\rangle$ and incorporating an additional normalization term into the definition of $p_w(t)$:

$$p_w(t) := \frac{|\langle w|\eta|\psi(t)\rangle|^2}{\langle\psi(0)|\Theta|\psi(0)\rangle}. \tag{A.22}$$

As before, $\{p_w(t)\}_w$ constitutes a valid probability distribution. Salimi and Sorouri [45] interpreted $p_w(t)$ as the transition probability of PHCTQW at vertex w and the time t, and observed that this probability at certain vertices increases compared to that of the Hermitian case in some illustrative examples. They envisioned that such a property could potentially accelerate the transport process and might be useful for search algorithms.

B. Spectrum, evolution, and target probability for the non-Hermitian search model

In this section, we derive the first-maximum evolution time of our non-Hermitian search model, as presented in Eq. (7) of the main text. We first compute the eigenvalues and eigenvectors of the non-Hermitian Hamiltonian defined in Eq. (5), a crucial step in showing that it is pseudo-Hermitian. Then, we derive the explicit form of the output state after evolution time t, given the non-Hermitian Hamiltonian and the specific uniform superposition input state. Finally, we calculate the metric transition probability $p_w(t)$ for the target state $|w\rangle$ at time t.

Eigenvalues and eigenvectors of the non-Hermitian Hamiltonian. The non-Hermitian Hamiltonian H defined in Eq. (5) has the following eigenvalues and associated eigenvectors. Here $a_{p,j}$ are real, $a_{p,w} = 0$, and the vectors with $p = 3, \ldots, N$ form an orthonormal basis of the unmarked zero-sum subspace (empty for $N = 2$).

$$E_1 = 0, \quad |\psi_1\rangle = \sqrt{\sqrt{N}}\,|w\rangle\,, \tag{B.1a}$$

$$E_2 = g, \quad |\psi_2\rangle = \frac{\sqrt{\sqrt{N}}}{\sqrt{N\,(N-1)}}\left[(N-1)\,|w\rangle - \sum_{j\neq w}|j\rangle\right], \tag{B.1b}$$

$$E_p = N + g - 1, \quad |\psi_p\rangle = \sum_{j\neq w} a_{p,j}\,|j\rangle\,,$$
$$\sum_j a_{p,j} = 0, \quad \sum_j |a_{p,j}|^2 = 1, \quad \sum_j a_{p_1,j}a_{p_2,j} = \delta_{p_1p_2}, \quad p = 3, \cdots, N. \tag{B.1c}$$

Accordingly, the eigenvalues and eigenvectors of $H^\dagger$ are:

$$E_1 = 0, \quad |\phi_1\rangle = \frac{1}{\sqrt{\sqrt{N}}}\sum_j |j\rangle\,, \tag{B.2a}$$

$$E_2 = g, \quad |\phi_2\rangle = \frac{-\sqrt{\sqrt{N}}}{\sqrt{N-1}}\sum_{j\neq w}|j\rangle\,, \tag{B.2b}$$

$$E_p = N + g - 1, \quad |\phi_p\rangle = |\psi_p\rangle\,. \tag{B.2c}$$

The bases for the biorthonormal system of H and $H^\dagger$ are chosen as $\{|\psi_n\rangle\,, |\phi_n\rangle\}_n$.

Recall that an operator is pseudo-Hermitian if and only if it possesses real eigenvalues and is diagonalizable. As previously shown, the eigenvalues of H are

indeed real. We now demonstrate that H is diagonalizable by proving the linear independence of its eigenvectors. We proceed by contradiction. Assume, to the contrary, that there exists a set of complex numbers $c_1, \cdots, c_N$, not all zero, such that

$$c_1 |\psi_1\rangle + c_2 |\psi_2\rangle + \sum_{p=3}^{N} c_p |\psi_p\rangle = 0. \tag{B.3}$$

Expanding this equation gives

$$c_1\sqrt{\sqrt{N}}\,|w\rangle + c_2\frac{\sqrt{\sqrt{N}}}{\sqrt{N(N-1)}}\left[(N-1)\,|w\rangle - \sum_{j\neq w}|j\rangle\right] + \sum_{p=3}^{N} c_p \sum_{j\neq w} a_{p,j}\,|j\rangle = 0. \tag{B.4}$$

Rearranging the elements by the basis vectors $\{|j\rangle\}_j$, we have

$$\left(c_1\sqrt{\sqrt{N}} + c_2\frac{\sqrt{N-1}}{\sqrt{\sqrt{N}}}\right)|w\rangle + \sum_{j\neq w}\left(-c_2\frac{\sqrt{\sqrt{N}}}{\sqrt{N(N-1)}} + \sum_{p=3}^{N} c_p a_{p,j}\right)|j\rangle = 0. \tag{B.5}$$

Since $\{|j\rangle\}_j$ is an orthonormal basis, all displayed coefficients vanish. Summing the unmarked coefficients and using $\sum_{j\neq w} a_{p,j} = 0$ gives $c_2 = 0$. The coefficient of $|w\rangle$ then gives $c_1 = 0$. Taking inner products with the orthonormal vectors $|\psi_p\rangle$ gives $c_p = 0$ for every $p \geq 3$, contradicting the assumption that the coefficients are not all zero. Thus, the set of vectors $\{|\psi_1\rangle, |\psi_2\rangle, ..., |\psi_N\rangle\}$ is linearly independent.

Output state after evolution time t. For the specific input uniform superposition state $|\psi(0)\rangle = \frac{1}{\sqrt{N}}\sum_{j=1}^{N}|j\rangle$, the corresponding normalized initial state in the non-Hermitian system can be calculated via Eq. (A.13) as

$$|\psi_0\rangle = \frac{|\psi(0)\rangle}{\sqrt{\langle\psi(0)|\Theta|\psi(0)\rangle}}. \tag{B.6}$$

We need to derive the explicit form of Θ. According to Eq. (A.6), it holds that

$$\Theta = \sum_n |\phi_n\rangle\langle\phi_n| = \frac{1}{\sqrt{N}}\sum_{j_1,j_2}|j_1\rangle\langle j_2| + \frac{\sqrt{N}}{N-1}\sum_{j_1\neq w, j_2\neq w}|j_1\rangle\langle j_2| + \sum_{p=3}^{N}\sum_{j_1\neq w, j_2\neq w} a_{p,j_1}a_{p,j_2}|j_1\rangle\langle j_2|. \tag{B.7}$$

Then we have

$$\sqrt{\langle\psi(0)|\Theta|\psi(0)\rangle} = \sqrt{\frac{2N-1}{\sqrt{N}}}, \quad |\psi_0\rangle = \frac{1}{\sqrt{(2N-1)\sqrt{N}}}\sum_{j=1}^{N}|j\rangle. \tag{B.8}$$

By Eq. (A.8), the state evolved from the metric-normalized input $|\psi_0\rangle$ after evolution time t is given by

$$\begin{aligned}|\psi(t)\rangle &= \sum_n e^{-iE_n t}|\psi_n\rangle\langle\phi_n|\psi_0\rangle \\ &= \frac{N}{\sqrt{(2N-1)\sqrt{N}}}|w\rangle + \frac{1}{\sqrt{(2N-1)\sqrt{N}}}e^{-igt}\left[(1-N)|w\rangle + \sum_{j\neq w}|j\rangle\right]. \end{aligned} \tag{B.9}$$

Note that $|\psi(t)\rangle$ above is the evolution of the metric-normalized input $|\psi_0\rangle$; the state evolved from the original uniform input $|\psi(0)\rangle$ is $e^{-iHt}|\psi(0)\rangle = \sqrt{\langle\psi(0)|\Theta|\psi(0)\rangle}\,|\psi(t)\rangle = \sqrt{\frac{2N-1}{\sqrt{N}}}\,|\psi(t)\rangle$. Because e^{-iHt} is not unitary, the ordinary norm of the output is not conserved; a direct calculation from Eq. (B.9) gives

$$\langle\psi(t)|\psi(t)\rangle = \frac{\sqrt{N}}{2N-1}\left[2N-1-2(N-1)\cos(gt)\right], \tag{B.10}$$

so that the ordinary norm of the physical output state is

$$\langle e^{-iHt}\psi(0)|e^{-iHt}\psi(0)\rangle = 2N-1-2(N-1)\cos(gt), \tag{B.11}$$

which equals $4N-3$ at $t=\pi/g$.

Metric probability at the target state $|w\rangle$. We now compute the metric transition probability $p_w(t)$ after evolution time t. This probability is determined by the inner product $\langle w|\eta|\psi(t)\rangle$. The eigenvalues and eigenvectors of Θ satisfy

$$\lambda_1 = \sqrt{N}+\sqrt{N-1},$$

$$|r_1\rangle = \frac{1}{\sqrt{2\sqrt{N}\left(\sqrt{N}+\sqrt{N-1}\right)}}|w\rangle + \frac{\sqrt{\sqrt{N}+\sqrt{N-1}}}{\sqrt{2(N-1)\sqrt{N}}}\sum_{j\neq w}|j\rangle, \tag{B.12a}$$

$$\lambda_2 = \sqrt{N}-\sqrt{N-1},$$

$$|r_2\rangle = \frac{1}{\sqrt{2\sqrt{N}\left(\sqrt{N}-\sqrt{N-1}\right)}}|w\rangle - \frac{\sqrt{\sqrt{N}-\sqrt{N-1}}}{\sqrt{2(N-1)\sqrt{N}}}\sum_{j\neq w}|j\rangle, \tag{B.12b}$$

$$\begin{aligned}&\lambda_p = 1, \quad |r_p\rangle = \sum_{j\neq w} a_{p,j}|j\rangle, \\ &\sum_j a_{p,j} = 0, \quad \sum_j |a_{p,j}|^2 = 1, \\ &\sum_j a_{p_1,j}a_{p_2,j} = \delta_{p_1p_2}, \quad p = 3,\cdots,N. \end{aligned} \tag{B.12c}$$

Since $\eta = \sqrt{\Theta}$, it follows that

$$\eta = \sqrt{\Theta} \tag{B.13}$$

$$= \frac{\sqrt{\sqrt{N}+\sqrt{N-1}}}{2\sqrt{N(N-1)}}\left(\sum_{j\neq w}|w\rangle\langle j| + \sum_{j\neq w}|j\rangle\langle w|\right)$$
$$+ \frac{\left(\sqrt{N}+\sqrt{N-1}\right)^{3/2}}{2(N-1)\sqrt{N}}\sum_{j_1\neq w, j_2\neq w}|j_1\rangle\langle j_2| \tag{B.14}$$
$$- \frac{\sqrt{\sqrt{N}-\sqrt{N-1}}}{2\sqrt{N(N-1)}}\left(\sum_{j\neq w}|w\rangle\langle j| + \sum_{j\neq w}|j\rangle\langle w|\right)$$
$$+ \frac{\left(\sqrt{N}-\sqrt{N-1}\right)^{3/2}}{2(N-1)\sqrt{N}}\sum_{j_1\neq w, j_2\neq w}|j_1\rangle\langle j_2| \tag{B.15}$$
$$+ \frac{1}{2\sqrt{N\left(\sqrt{N}+\sqrt{N-1}\right)}}|w\rangle\langle w| + \frac{1}{2\sqrt{N\left(\sqrt{N}-\sqrt{N-1}\right)}}|w\rangle\langle w|$$
$$+ \sum_{p=3}^{N}\sum_{j_1\neq w, j_2\neq w} a_{p,j_1}a_{p,j_2}|j_1\rangle\langle j_2|. \tag{B.16}$$

Based on the above expression of η, we compute the probability amplitude of the target state $|w\rangle$ as

$$\langle w|\eta|\psi(t)\rangle = \frac{N}{2\sqrt{(2N-1)N\sqrt{N}\left(\sqrt{N}+\sqrt{N-1}\right)}} + \frac{N}{2\sqrt{(2N-1)N\sqrt{N}\left(\sqrt{N}-\sqrt{N-1}\right)}} \tag{B.17a}$$

$$+ e^{-igt}\left(\frac{1-N}{2\sqrt{(2N-1)N\sqrt{N}\left(\sqrt{N}+\sqrt{N-1}\right)}} + \frac{\sqrt{(N-1)\left(\sqrt{N}+\sqrt{N-1}\right)}}{2\sqrt{(2N-1)N\sqrt{N}}}\right) \tag{B.17b}$$

$$+ e^{-igt}\left(\frac{1-N}{2\sqrt{(2N-1)N\sqrt{N}\left(\sqrt{N}-\sqrt{N-1}\right)}} - \frac{\sqrt{(N-1)\left(\sqrt{N}-\sqrt{N-1}\right)}}{2\sqrt{(2N-1)N\sqrt{N}}}\right) \tag{B.17c}$$

$$\equiv A + e^{-igt}B, \tag{B.17d}$$

where

$$A := \frac{N(\sqrt{(\sqrt{N}+\sqrt{N-1})}+\sqrt{(\sqrt{N}-\sqrt{N-1})})}{2\sqrt{(2N-1)\,N\sqrt{N}}}, \tag{B.18}$$

$$B := \frac{(1-N)\left(\sqrt{(\sqrt{N}+\sqrt{N-1})}+\sqrt{(\sqrt{N}-\sqrt{N-1})}\right)}{2\sqrt{(2N-1)\,N\sqrt{N}}} + \frac{\sqrt{N-1}\left(\sqrt{(\sqrt{N}+\sqrt{N-1})}-\sqrt{(\sqrt{N}-\sqrt{N-1})}\right)}{2\sqrt{(2N-1)\,N\sqrt{N}}}. \tag{B.19}$$

The transition probability to the target state $|w\rangle$ at the time t is then given by

$$\begin{aligned} p_w(t) = |\langle w|\eta|\psi(t)\rangle|^2 &= A^2 + B^2 + 2AB\cos(gt) \\ &= \frac{(2N-1)\sqrt{N}+1}{2\,(2N-1)\sqrt{N}} + \frac{1-N}{2N-1}\cos(gt)\,. \end{aligned} \tag{B.20}$$

In particular, $t = \pi/g$ gives the target state $|w\rangle$ with maximal probability

$$p_w(\pi/g) = \frac{4N\sqrt{N}-3\sqrt{N}+1}{2(2N-1)\sqrt{N}} = \Theta(1). \tag{B.21}$$

C. Spectrum, evolution, and target probability for the Hermitian counterpart

In this section, we derive the first-maximum evolution time of the Hermitian counterpart, as presented in Eq. (10) of the main text. We begin by explicitly computing the eigenvalues and eigenvectors of the Hermitian Hamiltonian $\tilde{H}$ defined in Eq. (8), which is constructed from the non-Hermitian Hamiltonian H. Then, we calculate the probability of measuring the system in the target state $|w\rangle$ at time t.

Eigenvalues and eigenvectors of the Hermitian Hamiltonian. Since $\tilde{H} = \eta H \eta^{-1}$, $\tilde{H}$ is similar to H, and they therefore share the same eigenvalues. Given an eigenvalue λ, let $|v\rangle$ and $|v'\rangle$ be corresponding eigenvectors, chosen consistently under the similarity transformation, of H and $\tilde{H}$, respectively. We have

$$\begin{aligned} & H|v\rangle = \lambda|v\rangle\,, \quad \tilde{H}|v'\rangle = \lambda|v'\rangle \\ & \Rightarrow H\eta^{-1}|v'\rangle = \lambda\eta^{-1}|v'\rangle \\ & \Rightarrow |v'\rangle = \eta|v\rangle\,. \end{aligned} \tag{C.1}$$

Then, from Eq. (B.1) we know that the eigenvalues and eigenvectors of the Hermitian Hamiltonian $\tilde{H}$ are given by

$$E_1 = 0, \quad |q_1\rangle = \eta|\psi_1\rangle\,, \tag{C.2a}$$

$$E_2 = g, \quad |q_2\rangle = \eta|\psi_2\rangle\,, \tag{C.2b}$$

$$E_p = N+g-1, \quad |q_p\rangle = \eta|\psi_p\rangle\,, \quad p = 3, \cdots, N. \tag{C.2c}$$

Interestingly, we can further prove that $|q_p\rangle = |\psi_p\rangle$ for all $p \geq 3$ as follows. Since $\Theta|\psi_p\rangle = |\psi_p\rangle$, its positive square root also fixes $|\psi_p\rangle$, so the vector equality has no phase ambiguity. Let $A = \sum_n |\phi_n\rangle\langle\phi_n|$ and $B = |\psi_p\rangle\langle\psi_p|$. Then A and B are positive semidefinite matrices by definition. We have

$$AB = \sum_n |\phi_n\rangle\langle\phi_n| \times |\psi_p\rangle\langle\psi_p| = |\phi_p\rangle\langle\psi_p|, \tag{C.3}$$

$$BA = |\psi_p\rangle\langle\psi_p| \times \sum_n |\phi_n\rangle\langle\phi_n| = |\psi_p\rangle\langle\phi_p|, \tag{C.4}$$

where we have used the biorthonormality property $\langle\psi_m|\phi_n\rangle = \delta_{mn}$. From Eq. (B.2) we know that $\forall p \geq 3, |\phi_p\rangle = |\psi_p\rangle$, and thus $|\phi_p\rangle\langle\psi_p| = |\psi_p\rangle\langle\phi_p|$. This means that $AB = BA$. Correspondingly,

$$\forall p \geq 3, \quad |q_p\rangle\langle q_p| = \eta|\psi_p\rangle\langle\psi_p|\eta^\dagger \tag{C.5}$$

$$= \sqrt{\sum_m |\phi_m\rangle\langle\phi_m|}\sqrt{|\psi_p\rangle\langle\psi_p|}\sqrt{|\psi_p\rangle\langle\psi_p|}\sqrt{\sum_n |\phi_n\rangle\langle\phi_n|} \tag{C.6}$$

$$= \sqrt{\sum_m |\phi_m\rangle\langle\phi_m| \times |\psi_p\rangle\langle\psi_p|} \times \sqrt{|\psi_p\rangle\langle\psi_p| \times \sum_n |\phi_n\rangle\langle\phi_n|} \tag{C.7}$$

$$= \sqrt{|\phi_p\rangle\langle\psi_p|}\sqrt{|\psi_p\rangle\langle\phi_p|} \tag{C.8}$$

$$= \sqrt{|\psi_p\rangle\langle\psi_p|}\sqrt{|\psi_p\rangle\langle\psi_p|} \tag{C.9}$$

$$= |\psi_p\rangle\langle\psi_p|, \tag{C.10}$$

where in the third equality we have used the following Lemma 1.

Lemma 1. *Let A and B be two positive semidefinite matrices of the same dimension. If $AB = BA$, then $\sqrt{A}\sqrt{B} = \sqrt{AB}$.*

Proof. We need to demonstrate that the matrix $X = \sqrt{A}\sqrt{B}$ is the unique positive semidefinite square root of the product AB. It suffices to show that X is positive semidefinite and $X^2 = AB$.

We first show that X is positive semidefinite. Since $AB = BA$, they are simultaneously diagonalizable by a unitary matrix U:

$$A = UD_AU^\dagger, \quad B = UD_BU^\dagger, \tag{C.11}$$

where D_A and D_B are diagonal matrices containing the non-negative real eigenvalues of A and B, respectively. Then, we can write X as

$$X = \sqrt{A}\sqrt{B} = U\sqrt{D_A}U^\dagger U\sqrt{D_B}U^\dagger = U\sqrt{D_AD_B}U^\dagger. \tag{C.12}$$

This form indicates that X is a positive semidefinite matrix, as it is unitarily equivalent to $\sqrt{D_AD_B}$.

We then show that $X^2 = AB$, which is evident since

$$X^2 = (\sqrt{A}\sqrt{B})(\sqrt{A}\sqrt{B}) = \sqrt{A}\sqrt{A}\sqrt{B}\sqrt{B} = AB, \tag{C.13}$$

where in the second equality we used the fact that when A and B are positive semidefinite, $AB = BA$ implies $\sqrt{A}\sqrt{B} = \sqrt{B}\sqrt{A}$. □

Probability at the target state $|w\rangle$. The spectral decomposition of the Hermitian operator $\tilde{H}$ is given by $\tilde{H} = \sum_p E_p |q_p\rangle\langle q_p|$. Then, the unitary evolution operator $U(t)$ satisfies:

$$U(t) = e^{-i\tilde{H}t} \tag{C.14}$$

$$= \sum_p e^{-iE_p t} |q_p\rangle\langle q_p| \tag{C.15}$$

$$= e^{-iE_1 t}\eta|\psi_1\rangle\langle\psi_1|\eta^\dagger + e^{-iE_2 t}\eta|\psi_2\rangle\langle\psi_2|\eta^\dagger + \sum_{p\geq 3} e^{-iE_p t}|\psi_p\rangle\langle\psi_p| \tag{C.16}$$

$$= \sqrt{N}\eta|w\rangle\langle w|\eta + e^{-i(N+g-1)t}\sum_{p\geq 3}\sum_{j_1\neq w, j_2\neq w} a_{p,j_1}a_{p,j_2}|j_1\rangle\langle j_2| \tag{C.17}$$

$$+ \frac{\sqrt{N}}{N(N-1)} e^{-igt}\Bigg[(N-1)^2\,\eta|w\rangle\langle w|\eta - (N-1)\sum_{j\neq w}\eta|w\rangle\langle j|\eta \tag{C.18}$$

$$- (N-1)\sum_{j\neq w}\eta|j\rangle\langle w|\eta + \sum_{j_1\neq w}\sum_{j_2\neq w}\eta|j_1\rangle\langle j_2|\eta\Bigg]. \tag{C.19}$$

For the initial state $|\psi(0)\rangle = \sum_{j=1}^N |j\rangle/\sqrt{N}$, we can calculate the probability amplitude at the marked vertex $|w\rangle$ as

$$\langle w|\tilde{\psi}(t)\rangle = \langle w|\,U(t)\,|\psi(0)\rangle \tag{C.20}$$

$$= \sum_j \langle w|\eta|w\rangle\langle w|\eta|j\rangle + e^{-igt}\Bigg[\frac{N-1}{N}\sum_j \langle w|\eta|w\rangle\langle w|\eta|j\rangle$$

$$- \frac{1}{N}\sum_{j_1\neq w,j}\langle w|\eta|w\rangle\langle j_1|\eta|j\rangle \tag{C.21}$$

$$- \frac{1}{N}\sum_{j_1\neq w,j}\langle w|\eta|j_1\rangle\langle w|\eta|j\rangle + \frac{1}{N(N-1)}\sum_{j_1\neq w, j_2\neq w, j}\langle w|\eta|j_1\rangle\langle j_2|\eta|j\rangle\Bigg] \tag{C.22}$$

$$= \frac{N+\sqrt{N}}{2N} + e^{-igt}\Bigg[\frac{-N^2 - N\sqrt{N} + \sqrt{N} + N}{2N^2}$$

$$+ \frac{\left(\sqrt{N}-1\right) + (N-1)\left(2\sqrt{N}-1\right)}{2N^2}\Bigg] \tag{C.23}$$

$$= \frac{N+\sqrt{N}}{2N} + e^{-igt}\frac{\sqrt{N}-N}{2N}. \tag{C.24}$$

Accordingly, the probability of observing the target state $|w\rangle$ at time t is given by

$$\tilde{p}_w(t) = |\langle w|\tilde{\psi}(t)\rangle|^2 = \frac{N+1}{2N} + \frac{1-N}{2N}\cos(gt). \tag{C.25}$$

In particular, $t = \pi/g$ yields the target state $|w\rangle$ with unit probability.